



## Original Article

# LOW-INTENSITY PULSED ULTRASOUND TARGETING FERROPTOSIS TO MITIGATE JOINT CAPSULE FIBROSIS IN A RAT MODEL OF POST-TRAUMATIC JOINT CONTRACTURE

X.L. Rao<sup>1,2,§</sup>, X.L. Kan<sup>1,§</sup>, C. Chen<sup>1,3</sup>, Y. Wang<sup>1</sup>, B.B. Zhang<sup>1,4</sup>, L. Sigdel<sup>5</sup>, J.N. Zhang<sup>1</sup>, J. Mao<sup>1</sup>, X.M. Li<sup>1</sup>, Q.B. Zhang<sup>1,\*</sup> and Y. Zhou<sup>1,\*</sup>

<sup>1</sup>Department of Rehabilitation Medicine, The Second Affiliated Hospital of Anhui Medical University, 230601 Hefei, Anhui, China

<sup>2</sup>Department of Rehabilitation Medicine, The First Affiliated Hospital of Anhui Medical University, Anhui Public Health Clinical Center, 230012 Hefei, Anhui, China

<sup>3</sup>Department of Orthopedics, Tongling People's Hospital, 244000 Tongling, Anhui, China

<sup>4</sup>Department of Rehabilitation Medicine, The First Affiliated Hospital of Bengbu Medical University, 233000 Bengbu, Anhui, China

<sup>5</sup>Department of Orthopedics, Bheri Hospital, 21900 Nepalgunj, Nepal

§These authors contributed equally.

## Abstract

**Background:** Post-traumatic joint contracture (PTJC) exhibits distinctive features such as excessive collagen deposition, which is the primary cause of joint capsule fibrosis. This work aimed to examine the therapeutic impacts and the fundamental mechanisms of low-intensity pulsed ultrasound (LIPUS) on PTJC-induced fibrosis, focusing on ferroptosis-related pathways. **Methods:** RNA sequencing (RNA-seq) data from the Gene Expression Omnibus (GEO) database were analyzed to identify differentially expressed genes (DEGs), followed by enrichment and correlation analyses. 40 Sprague-Dawley rats were separated into 5 groups: Sham, PTJC, Natural, LIPUS, and Combined. Rats in the LIPUS and Combined groups received LIPUS stimulation, while the Combined group also received erastin injections. Hematoxylin and Eosin (H&E) staining quantified inflammatory cell infiltration; Masson's trichrome staining measured collagen deposition. Immunofluorescence detected Cyclin D1 (fibroblast proliferation), phosphorylated nuclear factor kappa B (p-NF- $\kappa$ B) p65 (inflammation), solute carrier family 7 member 11 (*SLC7A11*)/glutathione peroxidase 4 (*GPX4*) (ferroptosis markers). Western blotting analyzed Collagen I/III, transforming growth factor beta 1 (TGF- $\beta$ 1)/Smad (fibrosis pathway). Range of motion (ROM) and joint diameter measurements evaluated contracture severity. **Results:** Bioinformatics analysis identified 17 ferroptosis-related and fibrosis-related target genes, with *SLC7A11* and *GPX4* selected for validation. ROM results indicated that LIPUS improved joint contracture more than the PTJC group, but the Combined group had less improvement than the LIPUS group alone. H&E and Masson's Trichrome staining partially reversing PTJC-induced inflammation and collagen deposition. Mechanistically, immunofluorescence and Western blot indicated that LIPUS reduced fibrosis by decreasing the proliferation-related (Cyclin D1) and inflammation-related protein (p-NF- $\kappa$ B p65), and LIPUS inhibited PTJC-mediated initiation of TGF- $\beta$ 1/Smad signalling pathway and prevented inactivation of the *SLC7A11*/*GPX4* axis. Erastin counteracted LIPUS effects, confirming ferroptosis involvement. **Conclusions:** These findings demonstrate that LIPUS significantly mitigates PTJC-induced joint capsule fibrosis by dual mechanisms: (1) activating the *SLC7A11*/*GPX4* axis to inhibit ferroptosis and (2) suppressing TGF- $\beta$ 1/Smad signaling. Ferroptosis-related factors were critical as their inhibition (via erastin) exacerbated fibrosis, highlighting their role in PTJC pathogenesis.

**Keywords:** Fibrosis, joint contracture, low-intensity pulsed ultrasound, ferroptosis, bioinformatics analysis.

**\*Address for correspondence:** Y. Zhou, Department of Rehabilitation Medicine, The Second Affiliated Hospital of Anhui Medical University, 230601 Hefei, Anhui, China. Email: [zhouyunanhuai@sina.com](mailto:zhouyunanhuai@sina.com); [zhoukeg@ahmu.edu.cn](mailto:zhoukeg@ahmu.edu.cn); Q.B. Zhang, Department of Rehabilitation Medicine, The Second Affiliated Hospital of Anhui Medical University, 230601 Hefei, Anhui, China. Email: [quanbingzhang@126.com](mailto:quanbingzhang@126.com).

**Copyright policy:** © 2025 The Author(s). Published by Forum Multimedia Publishing, LLC. This article is distributed in accordance with Creative Commons Attribution Licence (<http://creativecommons.org/licenses/by/4.0/>).

## Introduction

Post-traumatic joint contracture (PTJC)—a highly prevalent and challenging musculoskeletal sequela following articulation trauma as well as immobilisation—results in significant range of motion (ROM) loss, severely impairing mobility and quality of life. Approximately 3–18 % of patients suffer functional impairment post-tibial plateau fracture due to PTJC [1]. The pathogenesis of PTJC is generally attributed to two primary aetiologies: myogenic and arthrogenic contractures, with the latter being particularly critical in joint rehabilitation [2]. Arthrogenic contracture, characterised by joint capsule fibrosis, severely restricts joint function. Joint capsule fibrosis, which is marked by fibroblast proliferation, inflammatory infiltration, and excessive collagen deposition, is recognised as the primary barrier to joint mobility [3]. Animal studies support these observations, demonstrating progressive joint capsule fibrosis with extended immobilisation. This phenomenon has also been extensively documented in rabbit and rat models of knee extension contracture in our previous studies [4,5]. Therefore, alleviating joint capsule fibrosis and developing effective therapeutic interventions are crucial for the clinical treatment of PTJC.

Low-intensity pulsed ultrasound (LIPUS) is a biomechanical intervention that leverages acoustic cavitation and mechanotransduction mechanisms. LIPUS has emerged as a widely used non-invasive therapeutic modality in tissue regeneration and functional restoration in complex trauma cases [6]. Notably, LIPUS helps mitigate ROM restriction and reduces stiffness-related factors such as adhesions, decreased joint capsule elasticity, fibrosis, inflammation, and hypoxia after joint immobilisation [7]. Its effects on various cell types, including periodontal ligament cells, synoviocytes, and chondrocytes, have been well-documented, with benefits such as lowering inflammatory responses and improving hypoxic conditions [8–10]. Nakamura *et al.* [11] proposed that LIPUS exposure down-regulates cyclooxygenase-2 (COX-2) and prostaglandin E2 (PGE2) while upregulating hyaluronan synthase (HAS) 2 and HAS3 in interleukin-1 beta (IL-1 $\beta$ )-activated synovial membrane cells, thereby promoting an anti-inflammatory response. Our studies showed that LIPUS reduces knee joint capsule fibrosis by decreasing reactive oxygen species (ROS) and inhibiting the transforming growth factor beta 1 (TGF- $\beta$ 1)/Smad pathway, while Liao *et al.* [9] demonstrated its anti-fibrotic effects in osteoarthritis (OA) via the Wnt/ $\beta$ -catenin pathway [12]. Other studies have indicated that LIPUS alleviates renal fibrosis in experimental hypertensive and diabetic nephropathy models and lessens the cardiac fibrosis burden in cardiomyopathy [13,14]. However, the precise mechanisms underlying the effects of LIPUS on PTJC-related fibrosis have yet to be fully elucidated.

Ferroptosis, a specific type of programmed cell death, is supported by the weakening of antioxidant systems that rely on glutathione (GSH). This metabolic vulnerabil-

ity elicits a cascade of pathophysiological events, including iron-dependent lipid peroxidation (LPO), mitochondrial membrane potential collapse, and excessive reactive oxygen species (ROS) accumulation, collectively defining its unique morphological and biochemical signatures [15]. Emerging mechanistic insights reveal that ferroptosis is a pivotal modulator of fibrotic progression across diverse organ systems, including those affecting the lung, liver, heart, and kidneys [16–19]. The overproduction of lipid hydroperoxides initiates an inflammatory response, promoting fibroblast differentiation into myofibroblasts, which results in increased extracellular matrix (ECM) deposition and fibrogenesis [15,19]. The solute carrier family 7 member 11 (*SLC7A11*), acting as the catalytic component of the system Xc<sup>−</sup>, mediates cystine/glutamate antiport across the plasma membrane, a process critical for the progression of ferroptosis [20]. Once inside the cell, cystine is reduced to cysteine, which is utilised to synthesise the antioxidant GSH, thereby preventing ferroptosis induced by the accumulation of LPO. An emerging mechanistic study reveals that erastin, a prototypical ferroptosis inducer, drives fibroblast-to-myofibroblast transdifferentiation via glutathione peroxidase 4 (*GPX4*)-dependent lipid peroxidation amplification. Conversely, ferrostatin-1 (Fer-1) exhibits anti-fibrotic efficacy by enhancing *GPX4* and suppressing lipid peroxidation [21]. Another recent study has demonstrated that LIPUS effectively alleviates adriamycin-induced renal inflammation and fibrosis, ameliorates chronic kidney disease linked to oxidative stress and ferroptosis, and regulates the TGF- $\beta$ 1/Smad and nuclear factor erythroid 2-related factor 2 (Nrf2)/Kelch-like ECH-associated protein 1 (Keap1)/heme oxygenase-1 (HO-1) signalling pathways [22]. PTJC is a proliferative fibrotic condition induced by joint trauma and immobilisation, where fibroblast activation leads to excessive ECM production and deposition, contributing to joint capsule fibrosis. The TGF- $\beta$ 1/Smad pathway is a core driver of fibrosis in the PTJC joint capsule, promoting fibroblast activation, collagen deposition, and ECM remodeling. This pathway enhances lipid peroxidation by *Smad3*-dependent inhibition of *SLC7A11* transcription and upregulation of *ACSL4* expression, thereby exacerbating ferroptosis; ferroptotic products (such as 4-hydroxynonenal (4-HNE)) can feedback activate TGF- $\beta$ 1, forming a pro-fibrotic vicious cycle. However, the role of ferroptosis in PTJC-induced joint capsule fibrosis and the potential impact of LIPUS on this process are not well understood.

Although our previous study in rabbits demonstrated that LIPUS alleviates immobilization-induced fibrosis via TGF- $\beta$ 1/Smad inhibition [12], the present work advances this field by: (1) establishing a traumatic PTJC model in rats with distinct ferroptosis-related pathology, and (2) revealing that LIPUS exerts dual anti-fibrotic effects via *SLC7A11*/*GPX4* activation alongside TGF- $\beta$ 1/Smad suppression. These findings provide novel insights into PTJC-



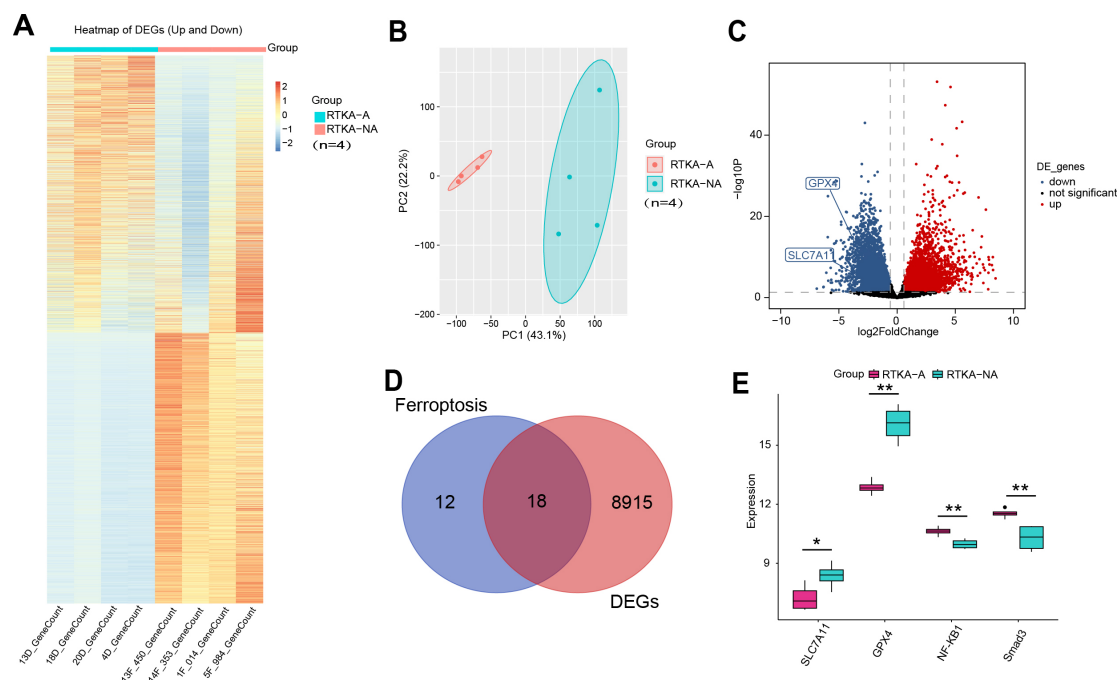


**Fig. 1. DEGs between RTKA-A (fibrosis) and RTKA-NA (non-fibrosis) samples in the GEO dataset.** (A) Heatmap of DEGs for GSE135854. (B) Principal component analysis (PCA) plot comparing gene expression profiles between RTKA-A and RTKA-NA samples (n = 4). (C) Volcano plot of DEGs for GSE135854. Blue color represents down-regulated genes, red color represents up-regulated genes, and black color represents genes that are not differentially expressed. (D) Venn diagram indicating overlap between ferroptosis-related as well as fibrosis-related DEGs. (E) Box plots depicting the expression levels of target genes (*SLC7A11*, *GPX4*, *NF-κB1*, *Smad3*). Data are expressed as mean ± SD. \* $p < 0.05$ , \*\* $p < 0.01$  between two specified groups. In the box-and-whisker plot, the black dot (•) in sub-figure E represents an outlier. Outliers are data points that deviate noticeably from the rest of the dataset. This dot indicates a value that is higher than the other observations within that group. Images were conducted in R (version 4.3.0) and GraphPad Prism 9 (version 9.2.0). GEO, Gene Expression Omnibus; DEGs, differentially expressed genes; *SLC7A11*, solute carrier family 7 member 11; *GPX4*, glutathione peroxidase 4; RTKA, Revision Total Knee Arthroplasty; SD, standard deviation.

specific therapeutic targets. Our study aimed to identify the key components and targets of PTJC, explore the therapeutic potential of LIPUS in PTJC-associated fibrosis, and investigate its underlying signalling pathways via bioinformatics analyses. Preliminary validation through animal experiments provided insights into the precise therapeutic targets of LIPUS and its multi-target effects in PTJC treatment.

## Materials and Methods

### Data Collection and Differentially Expressed Genes (DEGs) Analysis

We searched the Gene Expression Omnibus (GEO, <http://www.ncbi.nlm.nih.gov/geo>) database using the keywords “joint contracture” or “arthrofibrosis” with the following filters: “Homo sapiens” (biological) and “all arrays” (arrays). We selected the GSE135854 dataset, which contains four Revision Total Knee Arthroplasty (RTKA)-A (fibrotic), four RTKA-NA (non-fibrotic), and four Primary Total Knee Arthroplasty (PTKA) (non-post-traumatic fibrosis) samples. Since our study focused on post-traumatic fibrosis, PTKA samples were not included. The comparison between RTKA-A and RTKA-NA parallels our ex-

perimental study design of Sham vs. PTJC: RTKA-A—PTJC group: representing trauma-induced fibrosis; RTKA-NA—Sham group: serving as a control with minimal fibrosis. To investigate the differences between RTKA-A and RTKA-NA, we first performed principal component analysis (PCA) on the eight samples to detect outliers. Difference analysis was performed using the R 4.4.1 package (R Foundation for Statistical Computing, Vienna, Austria) “limma” for data normalization and differential expressed genes (DEGs). DEGs were screened according to the threshold  $|\log_2FC| > 0.585$ ,  $p$  value  $< 0.05$ , and DEGs were visualized using the package “ggplot2” (4.3.2, R Foundation for Statistical Computing, Vienna, Austria) to generate volcano plot and heat map. Based on a previous study to obtain 30 ferroptosis genes intersected with differential gene fetching, Venn diagrams (<http://bioinformatics.psb.ugent.be/webtools/Venn/>) were utilized to identify overlaps iron mutation-related genes and fibrosis-related DEGs, highlighting potential therapeutic targets [23]. In addition, box plots were generated to illustrate the expression levels of target genes.

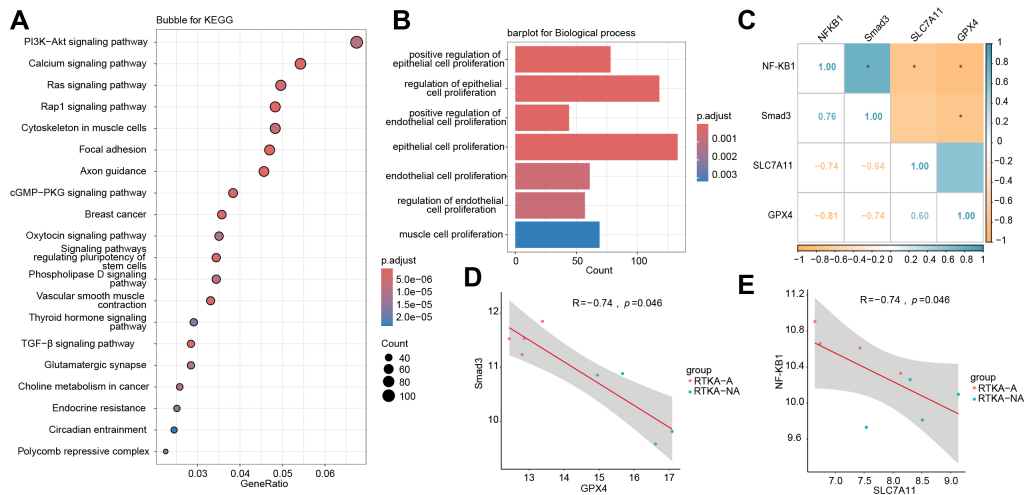


**Fig. 2. Enrichment and correlation analyses of ferroptosis-related and fibrosis-related DEGs between RTKA-A (fibrosis) and RTKA-NA (non-fibrosis) samples in the GEO dataset.** (A) KEGG enrichment analysis of fibrosis-related genes. The x-axis indicates the rich factor, while the y-axis denotes KEGG pathway names. (B) GO enrichment analysis of fibrosis-related genes. The x-axis represents the number of genes enriched in each term. (C) Correlation analysis between ferroptosis-related and fibrosis-related genes. (D) Scatter plot analysis between *GPX4* and *Smad3*. (E) Scatter plot analysis between *SLC7A11* and *NF-κB1*. Data are expressed as mean  $\pm$  SD. \* $p < 0.05$ , between two specified groups. Images were conducted in R (version 4.3.0) and GraphPad Prism 9 (version 9.2.0). GO, Gene Ontology; KEGG, Kyoto Encyclopedia of Genomes; TGF- $\beta$ , transforming growth factor-beta; PI3K-Akt, phosphoinositide 3-kinase-protein kinase B; Ras, rat sarcoma viral oncogene; Rap1, Ras-associated protein 1; cGMP-PKG, cyclic guanosine monophosphate-protein kinase G.

### Enrichment and Correlation Analyses

To delve deeper into the biological roles of crossover genes. We performed Gene Ontology (GO) and Kyoto Encyclopedia of Genomes (KEGG) enrichment analysis using the clusterProfiler package in R (3.6.3, R Foundation for Statistical Computing, Vienna, Austria), the ggplot2 package, and the significance threshold was set at  $p < 0.05$ . Bar plots were generated to illustrate the functional enrichment of the differential genes between RTKA-A and RTKA-NA in the GSE135854 dataset. The Spearman algorithm was applied to analyze the correlation of DEGs with genes associated with arthrocystic fibrosis, and the results were visualized using the ggplot2 software package in R.

### Animals and PTJC Model

Forty male Sprague-Dawley rats, aged 3 months, weighing 250–300 g, were purchased from the Experimental Animal Center of Anhui Medical University (Hefei, China). The rats were housed under controlled conditions at 24–25 °C with a 12-hour light/dark cycle, and were allowed unrestricted access to standard food and water. Then, we assigned them randomly to five groups with equal numbers of animals per group: (1) sham surgery (Sham), (2) post-traumatic joint contracture (PTJC) model, (3) naturally recovering for 4 weeks after PTJC induction (Natural), (4) low-intensity pulsed ultrasound (LIPUS) therapy, and (5) combined LIPUS and erastin intervention (Combined). Anesthesia was administered via intraperitoneal injection (2 % sodium pentobarbital, 40 mg/kg) across PTJC,

Natural, LIPUS, and Combined groups. PTJC surgery was conducted following our previously established protocol [24]: A 1.5 cm cut was created in the outer side of the left knee joint, and the kneecap was revealed by pressing it inward through the lateral parapatellar technique. The knee was bent to bring the femoral condyle into view, and a 1.2  $\times$  4 mm bone passage was drilled on both the outer and inner femoral condyles using a 1.2-mm bit. Ultimately, the kneecap was repositioned, and the wound was stitched up. The left knee joint was immobilized using an aluminum clamp, and the immobilization was maintained for 4 weeks with a full-extension fixation device (Patent No. 202120470158.0), as previously described [5]. In the sham group, only a skin incision was made following anesthesia, with no treatment to the joint capsule or joint immobilization.

### Intervention Methods

The safety and well-being of the immobilized rats were monitored daily. In the sham group, rats were allowed unrestricted movement in their cages for 8 weeks before euthanasia. Rats in the PTJC group were euthanized post-brace removal. Natural group rats underwent 4 weeks of cage activity post-removal before euthanasia. Euthanasia was induced by intraperitoneal sodium pentobarbital overdose (120 mg/kg), followed by hip joint disarticulation. LIPUS group rats received 4-week LIPUS intervention following brace removal. Combined group rats first received peritoneal administration of erastin

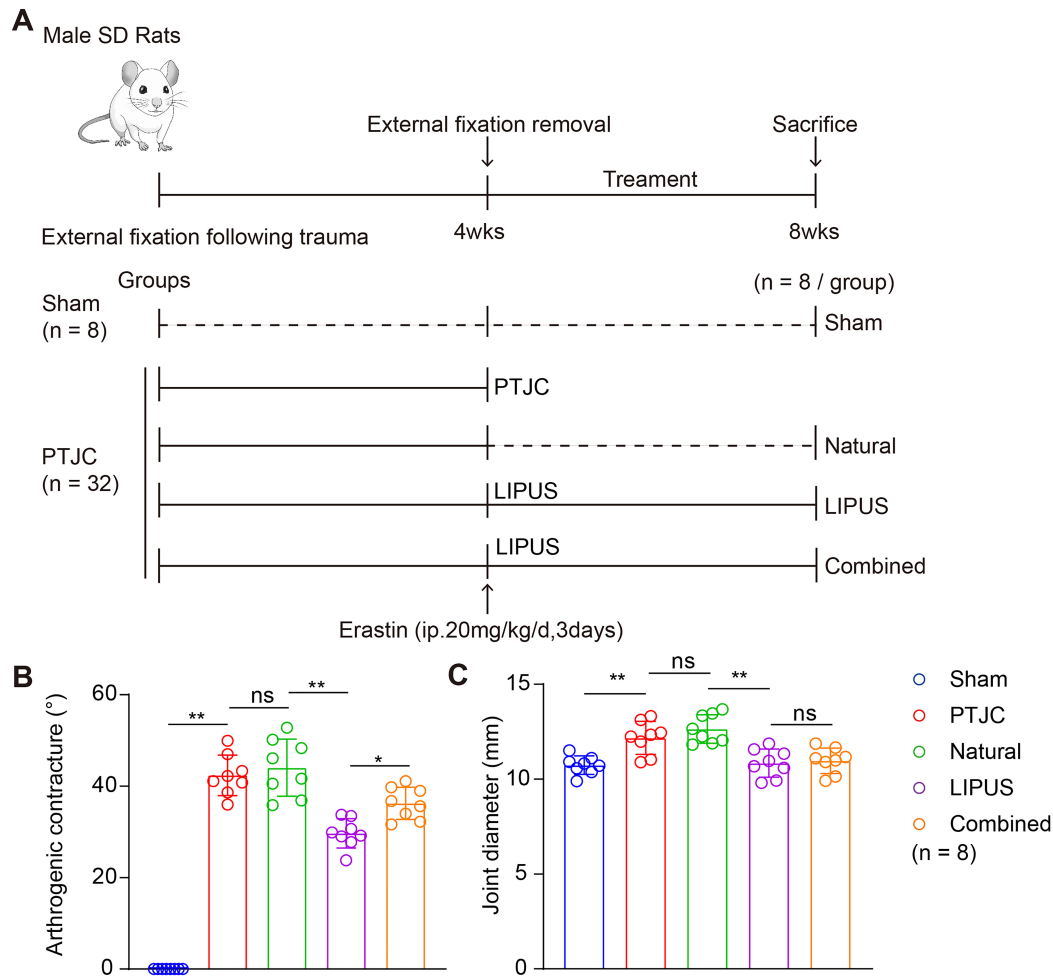


**Fig. 3. LIPUS ameliorates arthrogenic contracture.** (A) Schematic flowchart of experimental groups and intervention methods. (B) Changes in the degree of arthrogenic contracture. (C) Changes in the diameter of the knee. Data are expressed as mean  $\pm$  SD (n = 8). \* $p$  < 0.05, \*\* $p$  < 0.01, ns: no significant difference between two specified groups. Images were conducted in GraphPad Prism 9 (version 9.2.0). PTJC, post-traumatic joint contracture; LIPUS, low-intensity pulsed ultrasound.

(20 mg/kg/day for 3 days; dissolved in dimethyl sulfoxide (DMSO), with a final DMSO concentration of 10 % (v/v) in phosphate-buffered saline (PBS); KKL Med, Inc., KM9100, Guangzhou, China) and subsequently underwent 4-week LIPUS treatment [25]. LIPUS was administered using a device (2776, DJO, Chattanooga, TN, USA) (frequency: 1 MHz, intensity: 0.1 W/cm<sup>2</sup>) [12]. To minimize ultrasound energy loss, the left knee was shaved to remove fur, and ultrasound coupling gel was applied to both sides of the knee joint to ensure optimal acoustic transmission. Treatments consisted of daily 20-minute sessions, conducted 5 times weekly for a total duration of 4 weeks. After each treatment, the gel was wiped off, and the rats were placed back in their cages.

#### Knee Joint Diameter and ROM Measurement

Pre-euthanasia knee joint diameters were assessed via vernier caliper measurement in rats across groups, quantifying the horizontal distance between bilateral knee joint peaks at 90° flexion and full extension. Knee joint ROM

was assessed via a custom joint mobility meter developed by our research team (Patent No. ZL202120996643.1, knee measurement tool patent holder, Hefei, China). In this procedure, a longitudinal Kirschner wire insertion into the femur was followed by femur and lower limb fixation to a dial mechanism via adjustable clamping. During measurement, the electromagnet's mobile base and clamp height were adjusted to ensure that the femur was positioned correctly for optimal measurement. The device was then activated by rotating a handwheel, which caused the scale to move, and the dial to rotate accordingly. The rotation angle of the dial was tracked by a pointer, while the associated rotational force was recorded with a dynamometer calibrated to a standard torque of 0.053 N·m. The arthrogenic contracture was calculated using the following formula: Arthrogenic contracture angle = post-myotomy ROM of the right knee – post-myotomy ROM of the contracted knee.

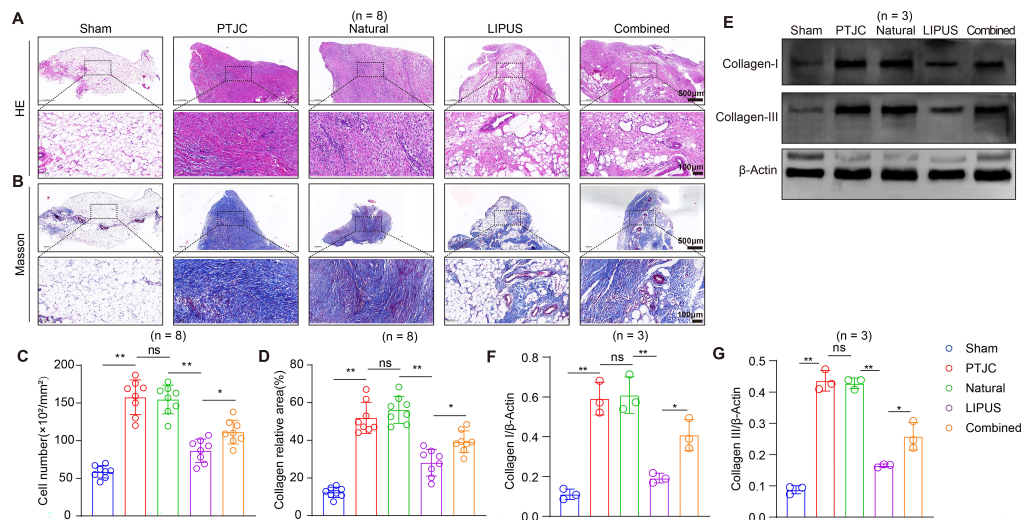


**Fig. 4. LIPUS alleviates pathological changes and reduces collagen deposition in the PTJC model joint capsule.** (A) H&E staining results. (B) Masson staining results. (C,D) Quantitative analysis of total cell count and collagen area percentage, with collagen stained blue, in each group (n = 8). (E–G) Western blot analysis and quantification of collagen I and III protein expression levels in the joint capsule in each group (n = 3). Data are expressed as mean  $\pm$  SD. \* $p$  < 0.05, \*\* $p$  < 0.01, ns: no significant difference between two specified groups. Scale bars: upper panel, 500  $\mu$ m; lower panel, 100  $\mu$ m. Images were conducted in Adobe Illustrator (version 2020) and GraphPad Prism 9 (version 9.2.0). H&E, Hematoxylin and Eosin.

#### Transmission Electron Microscopy

Joint capsule tissues were immobilized in 2.5 % glutaraldehyde (0.1 M phosphate buffer, P885738, Macklin, Shanghai, China) at 4 °C overnight. After incubation at 4 °C for 6–8 hours, the samples were sectioned into 1-mm<sup>3</sup> coronal slices. The samples were then fixed in phosphate buffer containing 1 % OsO<sub>4</sub> at 4 °C for 2 hours and thoroughly rinsed with double-distilled water (ddH<sub>2</sub>O). For en bloc staining, the samples were treated with 2 % aqueous uranyl acetate for 2 hours. Following staining, the samples were serially dehydrated through 50 %, 70 %, 90 %, and 100 % ethanol, followed by 100 % acetone, and then embedded in epoxy resin for block preparation. Silver sections were cut to a thickness of 70–90 nm using an ultramicrotome (EM UC7, Leica Microsystems, Wetzlar, Hesse, Germany) and stained with lead citrate and uranyl acetate. Finally, the sections were examined under an electron microscope (Talos L120C G2, Thermo Scientific, Waltham, MA, USA).

#### H&E and Masson Staining

Following ROM measurement, the anterior joint capsule of the left knee was excised and divided into uniform samples. A portion of the tissue was fixed in 4 % paraformaldehyde at 4 °C for 24 hours, then sectioned into 6  $\mu$ m slices using a microtome, deparaffinized, and stained with Hematoxylin and Eosin (H&E) and Masson's Trichrome (G1346, Beijing SolarBio Technology Co., Ltd, Beijing, China) to evaluate pathological alterations (cell counts, collagen deposition). H&E procedure includes: (1) Deparaffinization and hydration: Immerse slides in xylene

(2  $\times$  5 min) (10023418, Sinopharm Chemical Reagent Co., Ltd., Zhuhai, China), 100 % ethanol (2  $\times$  3 min) to 95 % to 70 % ethanol (1 min each) (10009218, Sinopharm Chemical Reagent Co., Ltd., Zhuhai, China), and distilled water. (2) Stained with hematoxylin (nuclei, 3 min) (BA-4041, Baso Biotechnology Co., Ltd., Zhuhai, China) and eosin (cytoplasm, 1 min) (BA-4022, Baso Biotechnology Co., Ltd., Zhuhai, China). (3) Differentiation, dehydration, clearing, and mounting. Masson staining procedure is: (1) Deparaffinization and hydration: Same as H&E steps. (2) Staining: Hematoxylin (1 min), Biebrich Scarlet/Acid Fuchsin (5 min), Phosphomolybdic/Phosphotungstic Acid (5 min, decolorizes cytoplasm), and Aniline Blue (5 min, stains collagen blue). (3) Differentiation, dehydration, clearing, and mounting.

Stained sections were analyzed using a microscope (BX43F, Olympus, Tokyo, Japan) at 200 $\times$  magnification. Six random fields per section were photographed and analyzed to quantify cell numbers and collagen deposition. The joint capsule's cellular components mainly consisted of fibroblasts and inflammatory cells, identified by their morphology. Collagen deposition was evaluated by measuring the percentage of blue-stained areas within the tissue.

#### Immunofluorescence Staining

Paraffin-embedded joint capsule sections were deparaffinized by sequentially passing through three changes of xylene, each for 15 min, followed by rehydration in graded ethanol solutions. After rehydration, the sections were washed with running tap water to remove residual alcohol. Antigen retrieval was performed by incubating the



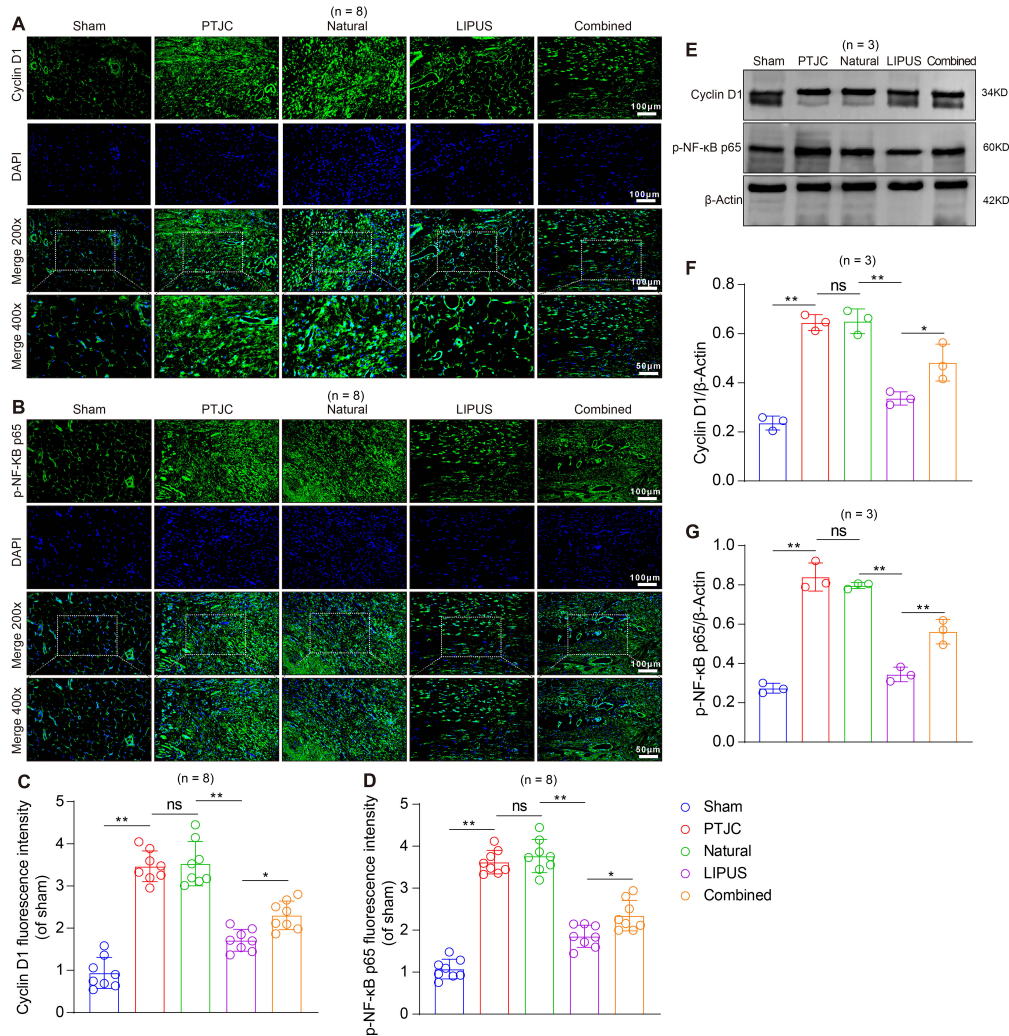


**Fig. 5. LIPUS inhibits proliferation and inflammation in the joint capsule in the PTJC model. (A,B)** Immunofluorescence staining showing fluorescence intensity changes of Cyclin D1 and p-NF- $\kappa$ B p65 in each group. **(C,D)** Fluorescence intensities of Cyclin D1 and p-NF- $\kappa$ B p65 were quantified using ImageJ software (U.S. National Institutes of Health, Bethesda, MD, USA) (n = 8). **(E–G)** Western blot analysis and quantification of Cyclin D1 and p-NF- $\kappa$ B p65 protein expression levels in the joint capsule in each group (n = 3). Data are expressed as mean  $\pm$  SD. \* $p$  < 0.05, \*\* $p$  < 0.01, ns: no significant difference between two specified groups. Scale bars: upper panel, 100  $\mu$ m; lower panel, 50  $\mu$ m. Images were conducted in Adobe Illustrator (version 2020) and GraphPad Prism 9 (version 9.2.0). p-NF- $\kappa$ B, phosphorylated nuclear factor kappa B; DAPI, 4',6-diamidino-2-phenylindole.

sections in ethylenediaminetetraacetic acid (EDTA) buffer (pH 8.0) in a pressure cooker, where they were heated for 2 min after the buffer reached a boil. Endogenous peroxidase activity was blocked by incubating the sections with 3 % hydrogen peroxide at room temperature for 20 min. The sections were incubated with primary antibodies as follows: anti-Cyclin D1 (1:500, AF0931, Affinity Biosciences, Jiangsu Qinke Biological Research Center Co., Ltd., Changzhou, China), anti-phosphorylated nuclear factor kappa B (p-NF- $\kappa$ B) p65 (1:200, AF2006, Affinity Biosciences, Jiangsu Qinke Biological Research Center Co., Ltd., Changzhou, China), anti-*SLC7A11* (1:500, DF12509, Affinity Biosciences, Jiangsu Qinke Biological Research Center Co., Ltd., Changzhou, China) and anti-TGF- $\beta$ 1 (1:500, BF8012, Affinity Biosciences, Jiangsu

Qinke Biological Research Center Co., Ltd., Changzhou, China) for 1 hour at 37 °C. After washing with PBS, the sections were incubated with a mixture of secondary antibodies: FITC Goat Anti-Rabbit IgG (H+L) (1:100, AS011, ABclonal Biotechnology Co., Ltd., Wuhan, China) and Cy3 Goat Anti-Mouse IgG (H+L) (1:100, AS008, ABclonal Biotechnology Co., Ltd., Wuhan, China) at 37 °C for 1 hour. 4',6-diamidino-2-phenylindole (DAPI) (C1002, Beyotime, Shanghai, China) staining was performed at room temperature for 5 min, followed by mounting with anti-fade medium. Images were captured using an automatic positive fluorescence microscope (DM6B; Leica, Wetzlar, Germany) at 400 $\times$  magnification, with subsequent quantification via ImageJ version 1.53c (U.S. National Institutes of Health, Bethesda, MD, USA).

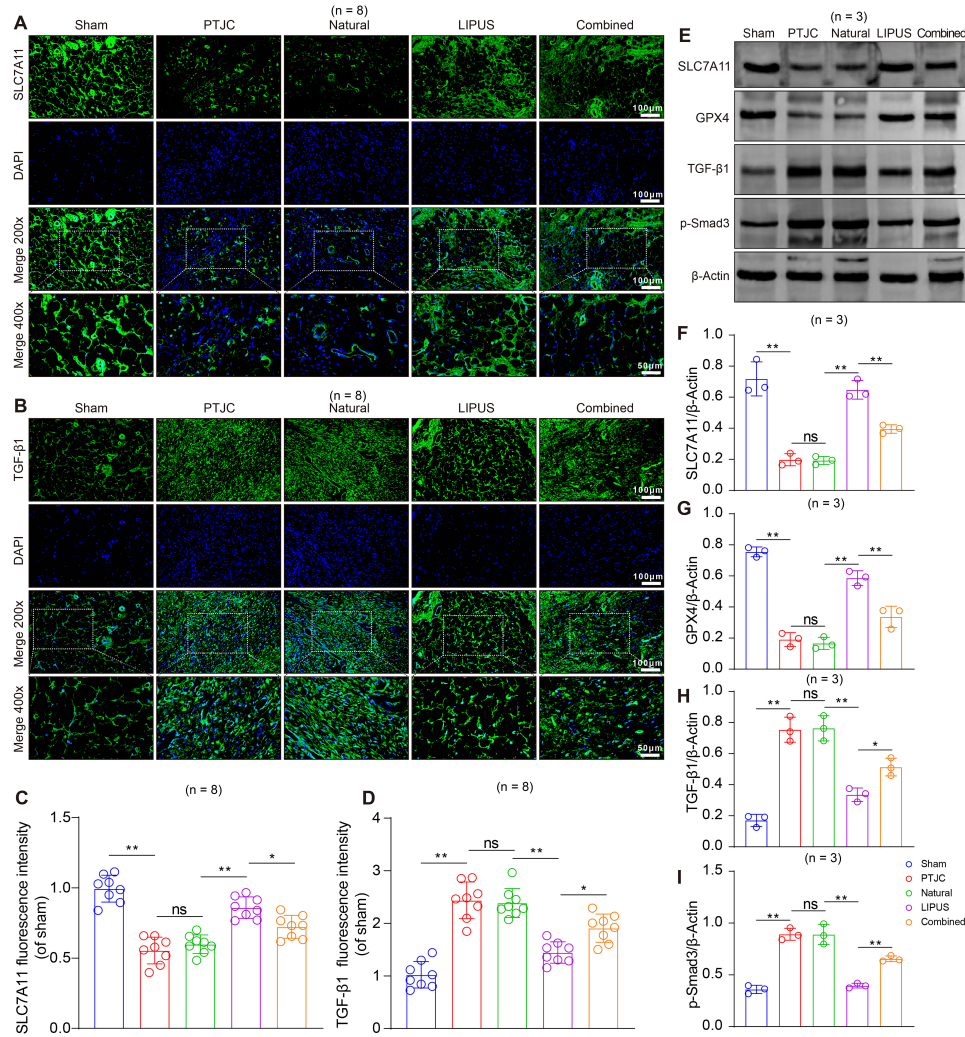


**Fig. 6. LIPUS inhibits the *SLC7A11*/GPX4 axis and the TGF- $\beta$ 1/Smad pathway in the joint capsule in the PTJC model. (A,B)** Immunofluorescence staining showing fluorescence intensity changes of *SLC7A11* and TGF- $\beta$ 1 in each group. **(C,D)** Fluorescence intensities of *SLC7A11* and TGF- $\beta$ 1 were quantified using ImageJ software (U.S. National Institutes of Health, Bethesda, MD, USA) ( $n = 8$ ). **(E–I)** Western blot analysis and quantification of *SLC7A11*, *GPX4*, TGF- $\beta$ 1, and p-*Smad3* protein expression levels in the joint capsule in each group ( $n = 3$ ). Data are expressed as mean  $\pm$  SD. \* $p < 0.05$ , \*\* $p < 0.01$ , ns: no significant difference between two specified groups. Scale bars: upper panel, 100  $\mu$ m; lower panel, 50  $\mu$ m. Images were conducted in Adobe Illustrator (version 2020) and GraphPad Prism 9 (version 9.2.0).

### Protein Extraction and Western Blotting

Tissue samples were homogenized into a fine powder using a liquid nitrogen grinder and lysed in radioimmunoprecipitation assay (RIPA) buffer (P0013B, Beyotime, Shanghai, China) supplemented with phenylmethylsulfonyl fluoride (PMSF) (ST505, Beyotime, Shanghai, China). The lysates were incubated on ice for 30 min to ensure complete lysis, followed by centrifugation to collect the supernatant. Protein concentration in the supernatant was performed via bicinchoninic acid (BCA) method (P0009, Beyotime, Shanghai, China). Equal amounts of protein (20  $\mu$ g per sample) were mixed with 5 $\times$  sodium dodecyl sulfate-polyacrylamide gel electrophoresis (SDS-PAGE) loading buffer (P0012A, Beyotime, Shanghai, China) and subjected to boiling for 10 min to in-

duce protein denaturation. Protein separation was conducted via SDS-PAGE, with subsequent electrotransfer of resolved proteins onto a polyvinylidene fluoride (PVDF) membrane (ISEQ00010, Millipore, Burlington, MA, USA) under constant current. The membrane underwent 2-hour incubation at room temperature in 5 % skim milk to minimize non-specific binding. After blocking, the membrane was washed with tris-buffered saline containing polysorbate 20 (TBST) and followed by overnight primary antibody incubation at 4  $^{\circ}$ C with the following targets: rabbit anti-collagen I (1:1000, AF7001, Affinity Biosciences, Jiangsu Qinke Biological Research Center Co., Ltd., Changzhou, China), rabbit anti-collagen III (1:1000, AF5457, Affinity Biosciences, Jiangsu Qinke Biological Research Center Co., Ltd., Changzhou, China), rabbit anti-



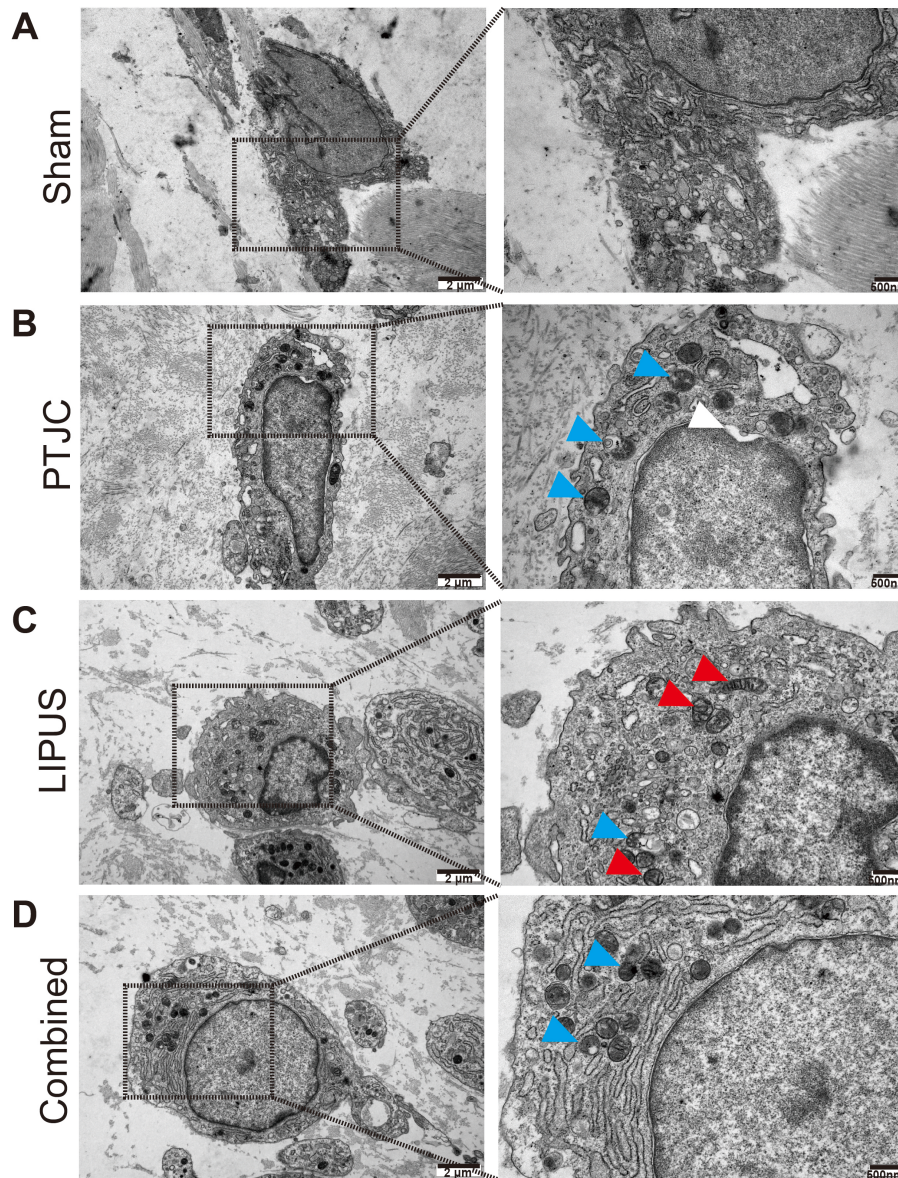


**Fig. 7. PTJC-induced ferroptosis of fibroblasts in the joint capsule.** (A) Representative transmission electron microscopy (TEM) image of a Sham rat. (B) Representative TEM image of a PTJC rat. (C) Representative TEM image of a LIPUS rat. (D) Representative TEM image of a Combined rat. Blue arrow: ruptured mitochondria; Red arrow: recovered mitochondria; white arrow: contracted cell nucleus. Scale bars: left panel, 2  $\mu\text{m}$ ; right panel, 500 nm. Images were conducted in Adobe Illustrator (version 2020).

Cyclin D1 (1:2000, AF0931, Affinity Biosciences, Jiangsu Qinke Biological Research Center Co., Ltd., Changzhou, China), rabbit anti-p-NF- $\kappa\text{B}$  p65 (1:2000, AF2006, Affinity Biosciences, Jiangsu Qinke Biological Research Center Co., Ltd., Changzhou, China), anti-TGF- $\beta$ 1 (1:2000, AF1027, Affinity Biosciences, Jiangsu Qinke Biological Research Center Co., Ltd., Changzhou, China), anti-p-Smad3 (1:2000, AF3362, Affinity Biosciences, Jiangsu Qinke Biological Research Center Co., Ltd., Changzhou,

China), anti-*SLC7A11* (1:2000, DF12509, Affinity Biosciences, Jiangsu Qinke Biological Research Center Co., Ltd., Changzhou, China), anti-*GPX4* (1:2000, DF6701, Affinity Biosciences, Jiangsu Qinke Biological Research Center Co., Ltd., Changzhou, China) and rabbit anti- $\beta$ -Actin (1:20000, AF7018, Affinity Biosciences, Jiangsu Qinke Biological Research Center Co., Ltd., Changzhou, China). The membrane underwent re-washing with TBST followed by 2-hour incubation at room temperature using

horseradish peroxidase (HRP)-conjugated secondary antibodies. Protein signals were detected via enhanced chemiluminescence (ECL) reagents (35050, Thermo Scientific, Waltham, MA, USA) and quantified using ImageJ version 1.53c (U.S. National Institutes of Health, Bethesda, MD, USA). Protein extraction was optimized for high-priority targets based on bioinformatics predictions.

### Statistical Analysis

All statistical analyses were performed using GraphPad Prism 9 (GraphPad Software, Inc., San Diego, CA, USA). Data are expressed as mean  $\pm$  standard deviation (SD) for each group. Prior to analysis, assumptions of normality and homogeneity of variances were assessed using the Shapiro-Wilk test and Levene's test (based on median), respectively. Differences between groups were evaluated using one-way analysis of variance (ANOVA), followed by post hoc comparisons with the Dunnett test for multiple comparisons. Statistical significance was defined as mean  $\pm$  SD; \* $p < 0.05$ , \*\* $p < 0.01$ .

## Results

### Identification of DEGs in Patients with Arthrogenic Fibrosis

From the GEO dataset, we identified 8933 DEGs, including 4517 upregulated and 4416 downregulated genes, as potential arthrogenic fibrosis targets and plotted heat maps and volcano maps (Fig. 1A,C). Fig. 1B shows the results of principal component analysis (PCA) comparing the gene expression profiles of RTKA-A (fibrotic) and RTKA-NA (non-fibrotic) samples. The results demonstrated that there were significant differences in gene expression patterns between the two groups of samples. Venn diagrams were generated by inputting the targets of iron metaplasia and fibrosis into the Venn diagram tool (Fig. 1D). We identified overlapping genes including *TF*, *FTMT*, *GPX4*, *SLC3A2*, *SAT1*, *MAP1LC3B*, *ATG7*, *SLC7A11*, *ACSL4*, *TFRC*, *VDAC2*, *GCLC*, *FTL*, *VDAC3*, *GSS*, *FTH1*, *HMOX1*, and *MAP1LC3A*. Of these, we chose genes of the classical iron-mutated pathway *SLC7A11/GPX4* axis as the target genes. Box plot results showed significant differences in the expression of target genes between RTKA-A and RTKA-NA samples (Fig. 1E).

### Enrichment and Correlation Analysis of Ferroptosis-Related and Fibrosis-Related DEGs

KEGG pathway analysis revealed significant enrichment of various pathways, such as phosphoinositide 3-kinase-protein kinase B (PI3K-Akt), rat sarcoma viral oncogene (Ras), Ras-associated protein 1 (Rap1), cyclic guanosine monophosphate-protein kinase G (cGMP-PKG), and TGF- $\beta$  signalling pathways (Fig. 2A). In addition, GO enrichment analysis using clusterProfiler identified seven pathways for epithelial cell proliferation, endothelial cell proliferation, and muscle cell proliferation, which were pre-

dominantly associated with fibrosis (Fig. 2B). Correlation analysis using the Spearman algorithm showed significant associations between the four target iron death-related and fibrosis-related DEGs (Fig. 2C). Specifically, scatter plot analysis demonstrated a moderate inverse correlation between *GPX4* and *Smad3*, as well as between *SLC7A11* and *NF- $\kappa$ B1*, in the GEO dataset (Fig. 2D,E).

### LIPUS Ameliorates Arthrogenic Contracture

The efficacy of LIPUS in mitigating PTJC-induced joint capsule fibrosis was evaluated via 4-week LIPUS intervention following model induction (Fig. 3A). ROM and knee diameter were measured as key indicators of joint contracture. Rats in the PTJC group exhibited significantly greater knee arthrogenic contracture (PTJC:  $42.38 \pm 4.44$  vs. Sham:  $0.00 \pm 0.00^\circ$ ;  $p < 0.01$ ) (Fig. 3B) and markedly larger knee diameters (PTJC:  $12.17 \pm 0.87$  mm vs. Sham:  $10.74 \pm 0.49$  mm;  $p < 0.01$ ) than those in the Sham group (Fig. 3C), indicating severe joint stiffness and swelling. To assess the impact of fixation removal, rats in the Natural group were allowed 4 weeks of recovery after external fixation. These rats showed no significant improvement in arthrogenic contracture (Natural:  $44.04 \pm 6.24$  vs. PTJC:  $42.38 \pm 4.44^\circ$ ;  $p = 0.92$ ) and demonstrated no significant recovery in knee diameter (Natural:  $12.64 \pm 0.76$  mm vs. PTJC:  $12.17 \pm 0.87$  mm;  $p = 0.68$ ). In contrast, rats treated with LIPUS after fixation removal showed improved knee arthrogenic contracture (LIPUS:  $29.69 \pm 3.19$  vs. Natural:  $44.04 \pm 6.24^\circ$ ;  $p < 0.01$ ) and significant improvement in knee diameter (LIPUS:  $10.84 \pm 0.74$  mm vs. Natural:  $12.64 \pm 0.76$  mm;  $p < 0.01$ ). The Combined group, however, exhibited poorer recovery in knee ROM than the LIPUS-only group (Combined:  $36.26 \pm 3.52$  vs. LIPUS:  $29.69 \pm 3.19^\circ$ ;  $p < 0.05$ ), with no significant differences in knee diameter between the two groups (Combined:  $10.97 \pm 0.67$  mm vs. LIPUS:  $10.84 \pm 0.74$  mm;  $p = 0.99$ ).

### LIPUS Alleviates Pathology and Reduces Collagen Deposition

The results of H&E staining are shown in Fig. 4A. The quantitative analysis (Fig. 4C) indicated that there was no statistically significant difference in the cell count between in the PTJC and Natural groups, however, the cell counts of PTJC group was significantly higher than in the Sham group ( $p < 0.01$ ). Qualitative evaluation of H&E-stained images revealed a notable increase in spindle-shaped fibroblasts and inflammatory cell infiltration in both the PTJC and Natural groups. Remarkably, the total cell count and inflammatory cell infiltration in the LIPUS group were significantly lower than in the Natural ( $p < 0.01$ ) and Combined groups ( $p < 0.05$ ), highlighting the efficacy of LIPUS in reducing cellular activity associated with inflammation and fibrosis in the PTJC model. Furthermore, the LIPUS group exhibited a significantly reduced cell count and inflammatory cell infiltration compared with the Combined group ( $p <$



0.05). The results of Masson staining are presented in Fig. 4B. Quantitative evaluation (Fig. 4D) revealed a significant increase in collagen deposition in the PTJC and Natural groups vs. the Sham group, there was no statistically significant difference in the collagen deposition between in the PTJC and Natural groups, however, the collagen deposition in the PTJC group was significantly higher than in the Sham group ( $p < 0.01$ ). Notably, the collagen deposition was significantly reduced in the LIPUS group relative to the Natural group ( $p < 0.01$ ). However, the Combined group exhibited significantly higher collagen levels than the LIPUS group ( $p < 0.05$ ). Western blot analysis of fibrosis-related proteins (collagen I/III) yielded consistent results, further corroborating these findings (Fig. 4E–G).

#### *LIPUS Inhibits Proliferation and Inflammation*

To investigate whether LIPUS inhibits fibroblast activation and proliferation, we assessed the expression levels of Cyclin D1, a proliferation-related protein, using immunofluorescence staining and Western blotting. As shown in Fig. 5A, PTJC induced significant fibroblast proliferation in the joint capsule, while LIPUS stimulation exerted a marked anti-proliferative effect. Quantitative analysis of the immunofluorescence staining revealed a significant increase in the fluorescence intensity of Cyclin D1 in both the PTJC and Natural groups relative to the Sham group, there was no statistically significant difference between in the PTJC and Natural groups, the fluorescence intensity of Cyclin D1 in the PTJC group was significantly higher than in the Sham group ( $p < 0.01$ ) (Fig. 5C). Furthermore, LIPUS treatment resulted in a significant reduction in Cyclin D1 fluorescence intensity relative to the Natural group ( $p < 0.01$ ). Notably, the fluorescence intensity of Cyclin D1 in the Combined group was significantly higher than in the LIPUS group ( $p < 0.05$ ). Similar results were observed for Western blot analysis of Cyclin D1 protein levels (Fig. 5E,F).

To investigate whether LIPUS inhibits inflammation in the joint capsule, we assessed the expression levels of the inflammation-related protein p-NF- $\kappa$ B p65 using immunofluorescence staining and Western blotting. As shown in Fig. 5B, PTJC induced a pronounced inflammatory response in the joint capsule, while LIPUS treatment exhibited a significant anti-inflammatory effect. Quantitative analysis of the immunofluorescence staining revealed a significant increase in p-NF- $\kappa$ B p65 fluorescence intensity in PTJC and Natural groups relative to the Sham group, there was no statistically significant difference between in the PTJC and Natural groups, the p-NF- $\kappa$ B p65 fluorescence intensity in the PTJC group was significantly higher than in the Sham group ( $p < 0.01$ ) (Fig. 5D). LIPUS intervention led to notable attenuation of p-NF- $\kappa$ B p65 fluorescence intensity relative to the Natural group ( $p < 0.01$ ). However, the Combined group exhibited elevated p-NF- $\kappa$ B p65 levels relative to LIPUS group ( $p < 0.05$ ). Western blot analysis

of p-NF- $\kappa$ B p65 protein levels yielded findings consistent with the above results (Fig. 5E,G).

#### *LIPUS Inhibits TGF- $\beta$ 1/Smad Pathway via the SLC7A11/GPX4 Axis*

To investigate whether LIPUS enhances the activation of the SLC7A11/GPX4 axis in the joint capsule, we evaluated SLC7A11 and GPX4 expression levels using immunofluorescence staining and Western blotting. Additionally, the Combined group was stimulated with erastin, a selective inhibitor of SLC7A11. The results indicated that the SLC7A11 fluorescence intensity was significantly reduced in the joint capsule of both the PTJC and Natural groups relative to the Sham group ( $p < 0.01$ ) (Fig. 6A,C). In contrast, the fluorescence intensity of SLC7A11 in the LIPUS group was significantly increased compared to the Natural group, suggesting that LIPUS promotes SLC7A11 expression in the joint capsule of PTJC rats. Western blot analysis demonstrated that PTJC suppressed the SLC7A11/GPX4 axis, as evidenced by a significant downregulation of SLC7A11 and GPX4 expression relative to the Sham group ( $p < 0.01$ ). However, LIPUS treatment resulted in increased expression of both SLC7A11 and GPX4 (Fig. 6E–G). In the Combined group, erastin treatment led to a further reduction in SLC7A11 and GPX4 levels relative to the LIPUS group ( $p < 0.01$ ), partially counteracting the protective effects of LIPUS against PTJC.

To investigate whether LIPUS inhibits the TGF- $\beta$ 1/Smad pathway in the joint capsule and its potential crosstalk with the SLC7A11/GPX4 axis, we assessed the expression of TGF- $\beta$ 1 and p-Smad3 proteins via immunofluorescence and Western blotting. Immunofluorescence analysis (Fig. 6B,D) revealed markedly elevated TGF- $\beta$ 1 fluorescence intensity in PTJC and Natural groups vs. the Sham controls ( $p < 0.01$ ). LIPUS intervention led to notable attenuation of TGF- $\beta$ 1 fluorescence relative to the Natural group ( $p < 0.01$ ). However, Combined group exhibited higher TGF- $\beta$ 1 fluorescence than the LIPUS group ( $p < 0.05$ ). Western blot profiling confirmed elevated TGF- $\beta$ 1/p-Smad3 expression in the PTJC/Natural groups vs. the Sham group ( $p < 0.01$ ), while the LIPUS group showed significant reduction in these markers compared with the Natural group ( $p < 0.01$ ) (Fig. 6E,H,I). In contrast, TGF- $\beta$ 1/Smad pathway protein expression levels remained elevated in the Combined group.

#### *PTJC-Induced Ferroptosis of Fibroblasts in the Joint Capsule*

Transmission electron microscopy results are presented in Fig. 7. In the Sham group, joint capsule tissue cells nuclei displayed regular morphology with uniformly distributed chromatin; mitochondria appeared intact with well-defined cristae, and the cell membrane remained unbroken (Fig. 7A). In contrast, fibroblasts from the PTJC group exhibited marked mitochondrial swelling, disrupted

cristae structure, and the formation of vacuoles. Nuclear condensation and chromatin marginalization were evident, along with compromised cell membrane integrity. Additionally, the accumulation of electron-dense granules was observed, indicative of ferroptosis-related pathological alterations (Fig. 7B). The transmission electron microscopy (TEM) results of the LIPUS group suggest that the cell nuclei have regular morphology, chromatin is more evenly distributed compared to the PTJC group, and there is a certain degree of recovery in mitochondrial integrity and cristae structure, with a significant reduction in the number of vacuolated mitochondria (Fig. 7C). In the combined group, the cell nuclei morphology appears regular with no significant changes compared to the LIPUS group; however, the number of swollen and vacuolated mitochondria has increased compared to the LIPUS group (Fig. 7D).

## Discussion

Following fractures or ligament injuries, joint immobilisation is typically required for a month or longer [26]. In this context, PTJC may be influenced by arthrogenic and myogenic components around the joint. Arthrogenic components include injuries to the bone, cartilage, capsule, and synovial membrane, while myogenic components involve lesions of the muscle, tendon, and fascia [4,27]. Arthrogenic components, particularly those related to the joint capsule, are critical contributors to PTJC-induced joint contracture [28]. The present results demonstrated that following 4 weeks of immobilisation, the left knee joint diameter in the PTJC group exhibited a statistically significant increase relative to the Sham group. However, after 4 weeks of unrestricted movement, the increased knee joint diameter did not return to baseline levels. As observed in our previous study, low activity levels of immobilised muscles lead to muscle atrophy [29]. However, in this study, the swollen joint capsule contributes to an increase in joint diameter. Similarly, post-fixation arthrogenic contracture angles were markedly elevated in PTJC group vs. Sham group. Notably, natural recovery for 4 weeks failed to alter the arthrogenic contracture angle in Natural group relative to PTJC group, indicating that unregulated mobility does not mitigate contracture severity—a conclusion corroborated by another prior study [30]. In this study, we applied LIPUS and observed its beneficial effects in reducing arthrogenic contracture induced by PTJC.

A previous study has shown that fibroblasts undergo excessive proliferation and migrate to the injury site, leading to excessive collagen deposition and, ultimately, to the formation of arthrofibrosis following TKA [31]. The results of GO enrichment analysis indicated a predominant association with biological processes related to cell proliferation. Fibroblasts and myofibroblasts are key effector cells in the pathogenesis of joint capsule fibrosis during contracture progression. During pathological fibrogenesis, activated fibroblasts drive ECM synthesis and collagen deposition, cul-

minating in dense fibrotic tissue formation. Pathological staining analysis of the anterior joint capsule revealed significantly elevated cellularity and collagen deposition in the PTJC group vs. the Sham group. Notably, natural recovery failed to alter fibrotic parameters, whereas LIPUS intervention significantly reduced both cellularity and collagen deposition, suggesting its therapeutic potential through fibrotic cell modulation and ECM remodelling. PTJC model rats exhibited pronounced fibroblast hyperplasia and upregulated expression of Cyclin D1, a key cell cycle regulator, underscoring fibroblast overactivation as a therapeutic target. LIPUS, a non-invasive modality that delivers precise mechanical stimuli, is widely adopted in clinical rehabilitation owing to its cost-effectiveness and targeted therapeutic potential [6,32]. However, the effects of LIPUS on cell proliferation have been inconsistent. Xu *et al.* [33] demonstrated LIPUS-mediated inhibition of preadipocyte proliferation via extracellular signal-regulated kinase (ERK)/p38 mitogen-activated protein kinase (MAPK) pathway modulation. In contrast, Duan *et al.* [34] demonstrated that LIPUS stimulates satellite cell proliferation and myogenic differentiation shortly after muscle injury, promoting the formation of new myotubes to replace damaged fibers and enhancing therapeutic efficacy over various durations. Another study, however, indicates that LIPUS has little effect on epithelial cell proliferation [35]. In our study, LIPUS suppressed fibroblast proliferation and Cyclin D1 expression.

TGF- $\beta$ 1 has emerged as a central mediator in fibrogenesis, orchestrating the activation of fibroblasts—the primary cellular component of the joint capsule. In a mouse skin fibrosis model, subcutaneous injection of TGF- $\beta$ 1 has been shown to sustain skin fibrosis [36]. A previous study has reported that platelet-rich plasma significantly reduces TGF- $\beta$ 1-induced activation of joint capsule fibroblasts and the expression of key fibrosis-related factors, such as TGF- $\beta$ 1,  $\alpha$ -smooth muscle actin ( $\alpha$ -SMA), collagen type I (COL-I), and matrix metalloproteinase-9 (MMP-9), likely through inhibition of the TGF- $\beta$ 1/Smad signalling pathway [37]. TGF- $\beta$ 1 is a versatile cytokine that regulates the expression of ECM-related genes during early injury [38]. This leads to the activation of collagen synthesis and secretion, particularly  $\alpha$ -SMA and collagen I/II genes and proteins, leading to renal and pulmonary fibrosis. Lei *et al.* [39] emphasised the regulatory role of LIPUS in modulating gene expression related to fibrosis. LIPUS has been documented to mitigate fibrotic remodeling via suppression of the TGF- $\beta$ 1/Smad/connective tissue growth factor (CTGF) axis in penile tissue. In this study, KEGG pathway analysis identified the enrichment of multiple signalling pathways, including the TGF- $\beta$  pathway. Additionally, prior investigation from our group has further established that LIPUS inhibits the TGF- $\beta$ 1/Smad signaling pathway and suppresses joint capsule fibrosis induced by immobilisation, notably reducing collagen I/III expression [12]. The

observed increase in collagen and fibrosis-related proteins in connective tissues is consistent with previous studies, which show elevated levels of collagen types I and III, as well as TGF- $\beta$ 1 and p-Smad3, after 4 weeks of immobilisation in the PTJC model. In contrast, both fibrosis-related proteins and collagen deposition were significantly reduced in the LIPUS group, suggesting that LIPUS mitigates joint capsule fibrosis by decreasing the levels of fibrosis-related proteins and collagen accumulation. These findings corroborate those of prior studies highlighting the anti-fibrotic properties of LIPUS in other musculoskeletal injury models, including osteoarthritis and renal fibrosis [13,40].

Joint trauma triggers oedema, bleeding, and an inflammatory response, during which resident and infiltrating immune and stromal cells are rapidly activated to secrete diverse cytokines and chemokines. Simultaneously, immobilisation induces joint capsule inflammation [41]. Inflammatory and proinflammatory signaling cascades triggered by trauma and immobilisation are pivotal factors in the development of joint contracture. Macrophages play a central role in these processes and exist in two primary phenotypic states: M1 and M2. The M1 phenotype is associated with proinflammatory effects, while M2 macrophages exhibit anti-inflammatory properties. LIPUS has been shown to accelerate tendon-bone interface repair by promoting a higher proportion of M2 macrophages and upregulating the messenger ribonucleic acid (mRNA) expression of anti-inflammatory genes [42]. Macrophages respond to a wide range of signals by secreting cytokines and chemokines and are closely associated with myofibroblasts [43]. TGF- $\beta$ 1 may enhance expression of profibrotic cytokines by activated macrophages, thus indirectly stimulating tissue fibroblast activation [44]. In this study, we observed that the number of inflammatory cells was significantly higher in the PTJC and Natural groups compared to the Sham group. Notably, LIPUS markedly reduced the inflammatory cell count in the PTJC group, suggesting its potential anti-inflammatory effects. Chronic inflammation perpetuates fibroblast activation and facilitates the recruitment of inflammatory cells, which release cytokines that amplify fibrotic signaling cascades [45]. The NF- $\kappa$ B family of transcription factors serves as pivotal regulators in inflammatory diseases. Elevated levels of p-NF- $\kappa$ B p65, a master regulator of inflammatory responses, were observed in PTJC animals, indicating persistent inflammatory activity. Overactivation of NF- $\kappa$ B contributes to fibrosis by inducing the expression of inflammatory cytokines and enhancing fibroblast survival [46]. By attenuating NF- $\kappa$ B activity, LIPUS likely disrupts the positive feedback loop between inflammation and fibrosis, thereby mitigating joint stiffness and alleviating pain.

Emerging research has revealed excessive iron accumulation as a hallmark of various fibrotic disorders. For instance, a significant accumulation of iron in lung tissue and altered expression of intracellular iron metabolism genes

promote pulmonary fibrosis by contributing to ferroptosis, mitochondrial dysfunction, and collagen deposition [47]. Similarly, another study has demonstrated that iron overload triggers ferroptosis in cardiac microvascular endothelial cells, contributing to heart dysfunction, cellular proliferation, migration, oxidative stress, myocardial hypertrophy, and fibrosis [19]. Furthermore, targeting ferroptosis has been identified as an effective strategy to mitigate renal fibrosis [48]. These findings underscore the critical role of ferroptosis as a pathological mechanism in fibrotic diseases. In our study, TEM revealed characteristic features of ferroptosis in rat joint capsule fibroblasts following 4 weeks of immobilization in the PTJC group. Observed changes included mitochondrial swelling, disruption of cristae structure, and vacuole formation, providing further evidence for the activation of ferroptosis in the context of joint capsule fibrosis.

The use of bioinformatics-driven high-throughput sequencing has become indispensable in biomedical research, facilitating advancements in disease diagnostics and precision medicine [49]. The identification of molecular biomarkers associated with joint capsule fibrosis is critical for enhancing early detection and diagnostic accuracy in PTJC. In this study, we leveraged transcriptomic profiling of joint capsule tissues from the GEO database to identify key regulatory genes implicated in fibrosis through differential expression analysis, enrichment, and gene correlation analyses. Eighteen differentially expressed genes (DEGs) related to both ferroptosis and fibrosis were identified, including *TF*, *FTMT*, *GPX4*, *SLC3A2*, *SAT1*, *MAP1LC3B*, *ATG7*, *SLC7A11*, *ACSL4*, *TFRC*, *VDAC2*, *GCLC*, *FTL*, *VDAC3*, *GSS*, *FTH1*, *HMOX1*, and *MAP1LC3A*. Among these are genes encoding proteins of the *SLC7A11*/*GPX4* axis, which is recognised as a classical regulator of ferroptosis and exhibits a negative correlation with inflammation and the TGF- $\beta$ 1/Smad signal pathway. In subsequent experiments, we further validated the expression of these target genes.

The *SLC7A11*/*GPX4* axis is a critical regulator within ferroptosis-related pathways. A previous study by Zhu *et al.* [50] demonstrated that enhancing *SLC7A11* expression alleviated ferroptosis, which otherwise triggers tubular atrophy and fibrosis. *GPX4*, with its unique anti-lipid peroxidation capacity, decomposes toxic LPO, thus preventing ferroptosis. Research by He *et al.* [51] indicated that silencing *GPX4* inhibits the protective effect of Fer-1 on vascular smooth muscle cell ferroptosis, while *in vivo* studies have demonstrated that Fer-1 alleviates Ang II-induced ferroptosis and vascular structural abnormalities in abdominal aortic aneurysm mice. Conversely, inhibition of *SLC7A11* diminishes GSH levels, reducing *GPX4* activity, increasing lipid peroxidation, and inducing ferroptosis [52]. Given the critical role of the *SLC7A11*/*GPX4* axis and our prior bioinformatics analysis, we assessed the expression levels of these molecules using Western blotting and immunofluorescence.



In the present study, protein levels of *SLC7A11* and *GPX4* were significantly lower in the PTJC group than the Sham group, indicating inactivation of the *SLC7A11*/*GPX4* axis following immobilisation and trauma. Notably, *SLC7A11* and *GPX4* levels were markedly elevated in the LIPUS group relative to the Natural and PTJC groups, suggesting that LIPUS may reactivate the *SLC7A11*/*GPX4* axis.

To further investigate whether LIPUS exerts its antifibrotic effects through the *SLC7A11*/*GPX4* axis, we conducted additional experiments. Erastin, first identified in 2003, is a compound known to induce ferroptosis and was initially used to screen for cancer drugs selectively targeting oncogenic Ras-mutant cell lines [53]. Erastin acts as a selective inhibitor of *SLC7A11*, blocking cystine uptake and consequently reducing intracellular cysteine levels. Sali-cylsulphonylpyrimidines and glutamate have similarly been shown to inhibit *SLC7A11*, leading to GSH depletion within cells [54]. In this study, although LIPUS treatment showed some inhibition of the TGF- $\beta$ 1/Smad signaling pathway, the inhibitory effect was much weaker when combined with erastin. In the LIPUS group, we observed significant reductions in fibrosis-related indicators, such as collagen deposition, fibroblast proliferation, and inflammation. However, following erastin treatment, these effects were reversed to varying degrees. Owing to experimental limitations, we were unable to perform gene expression level assays at the cellular level to further elucidate the underlying mechanisms.

It is necessary to acknowledge the limitations of this study. First, the use of a rat model may not fully capture the complexity of PTJC in humans, including the contributions of comorbidities and variability in patient responses. Second, the study's four-week duration limits the assessment of long-term therapeutic effects and the potential for fibrosis recurrence. Finally, while this study focused on the *SLC7A11*/*GPX4* axis, other pathways likely contribute to LIPUS-mediated fibrosis reduction and should be explored in future research. Considering the complexity of simulating the fibrotic microenvironment of the joint capsule *in vitro*, the next steps will involve: (a) using three-dimensional (3D) bioprinted joint capsule tissue models; (b) employing *SLC7A11* conditional knockout mice to further validate the hierarchical relationship between the *SLC7A11*/*GPX4* axis and the TGF- $\beta$ 1/Smad pathway. Besides, Further detection of lipid peroxidation products or iron ion levels directly demonstrates the role of ferroptosis in PTJC fibrosis is needed. Future studies should also investigate the optimal parameters for LIPUS therapy, including intensity, frequency, and duration, to maximize its therapeutic efficacy. Additionally, combining LIPUS with pharmacological inhibitors of fibrosis, such as TGF- $\beta$  or NF- $\kappa$ B antagonists, may further enhance its anti-fibrotic effects and improve functional outcomes. In summary, our findings demonstrate that LIPUS mitigates PTJC severity at morphological, histological, and molecular levels. This

therapeutic effect is likely mediated by the activation of the *SLC7A11*/*GPX4* axis and the regulation of the TGF- $\beta$ 1/Smad signaling pathway, potentially mitigating joint fibrosis by suppressing inflammation and fibroblast proliferation while inhibiting ferroptosis within the fibrotic joint capsule.

## Conclusions

In conclusion, this study provides novel mechanistic insights into the therapeutic effects of LIPUS on joint capsule fibrosis in PTJC. LIPUS effectively mitigates fibrosis by suppressing fibroblast proliferation and inflammation while modulating the *SLC7A11*/*GPX4* axis, thereby down-regulating the TGF- $\beta$ 1/Smad pathway. These findings highlight ferroptosis-related pathways as potential therapeutic targets for alleviating arthrogenic fibrosis.

## List of Abbreviations

PTJC, post-traumatic joint contracture; ROM, range of motion; LIPUS, low-intensity pulsed ultrasound; COX-2, cyclooxygenase-2; PGE2, prostaglandin E2; ROS, reactive oxygen species; OA, osteoarthritis; GSH, glutathione; LPO, lipid peroxidation; ECM, extracellular matrix; *GPX4*, glutathione peroxidase 4; *SLC7A11*, solute carrier family 7 member 11; Fer-1, ferrostatin-1; DEGs, differentially expressed genes; GEO, Gene Expression Omnibus; GO, Gene Ontology; KEGG, Kyoto Encyclopedia of Genomes; RNA-seq, RNA sequencing; H&E, Hematoxylin and Eosin; RTKA, Revision Total Knee Arthroplasty; PTKA, Primary Total Knee Arthroplasty; PCA, principal component analysis; SD, standard deviation; ddH<sub>2</sub>O, double-distilled water; RIPA, radioimmunoprecipitation assay; PMSF, phenylmethylsulfonyl fluoride; BCA, bicinchoninic acid; SDS-PAGE, sodium dodecyl sulfate-polyacrylamide gel electrophoresis; PVDF, polyvinylidene fluoride; TBST, tris-buffered saline containing polysorbate 20; HRP, horseradish peroxidase; ECL, enhanced chemiluminescence; ANOVA, analysis of variance; TEM, transmission electron microscopy; p-NF- $\kappa$ B, phosphorylated nuclear factor kappa B; Nrf2, nuclear factor erythroid 2-related factor 2; Keap1, Kelch-like ECH-associated protein 1; HO-1, heme oxygenase-1; 4-HNE, 4-hydroxynonenal; IL-1 $\beta$ , interleukin-1 beta; TGF- $\beta$ , transforming growth factor-beta, PI3K-Akt, phosphoinositide 3-kinase-protein kinase B; Ras, rat sarcoma viral oncogene; Rap1, Ras-associated protein 1; cGMP-PKG, cyclic guanosine monophosphate-protein kinase G; DAPI, 4',6-diamidino-2-phenylindole;  $\alpha$ -SMA, alpha-smooth muscle actin; COL-I, collagen type I, MMP-9, matrix metalloproteinase-9, CTGF, connective tissue growth factor; 3D, three-dimensional; DMSO, dimethyl sulfoxide; PBS, phosphate-buffered saline; EDTA, ethylenediaminetetraacetic acid.



## Availability of Data and Materials

The datasets used and analyzed during the current study are available from the first author on reasonable request. All data generated or analyzed during this study are included in this published article. The manuscript, including related data, and figures have not been previously published and are not under consideration elsewhere.

## Author Contributions

XLR and XLK contributed to the design of this work. CC, YW, BBZ, LS, JNZ, and JM contributed to the interpretation of data. XLR, XLK, and XML analyzed the data. QBZ and YZ revised critically for important intellectual content. All authors read and approved the final manuscript. All authors agreed to be accountable for all aspects of the work in ensuring that questions related to the accuracy or integrity of any part of the work were appropriately investigated and resolved.

## Ethics Approval and Consent to Participate

Animal care and experimental procedures were performed in accordance with the Guidelines for Animal Experimentation of Anhui Medical University and were approved by the Institutional Animal Care and Use Committee (LLSC20241419).

## Acknowledgments

We are very grateful for the guidance and help from associate professor Hua-Long Zhu from the School of Public Health, Anhui Medical University and Professor Bin Li from Soochow University.

## Funding

This work was supported by Anhui Medical University School Foundation (2022XKJ061), Health Research Program of Anhui (AHWJ2022b063), Anhui Provincial Natural Science Foundation (2408085QH270), Key Natural Science Research Project of Anhui Educational Committee (2024AH050788), Key Scientific Research Project Fund of Wannan Medical Colleges (WK2023JXYY121), National Natural Science Incubation Program of the Second Hospital of Anhui Medical University (2022GMFY05), Summit Discipline Construction Project of Anhui Medical University (Clinical Medicine) in 2022 (2022GFXK-EFY08), Clinical Medicine Discipline Construction Project of Anhui Medical University in 2023 (2023LCXKKEFY010), Health Research Program of Anhui (AHWJ2023A30077) and Research Fund of Anhui Institute of Translational Medicine (2023ZHYX-C85).

## Conflict of Interest

The authors declare no conflict of interest, financial or otherwise.

## References

- [1] Gálvez-Sirvent E, Ibarzábal-Gil A, Rodríguez-Merchán EC. Complications of the surgical treatment of fractures of the tibial plateau: prevalence, causes, and management. *EFORT Open Reviews*. 2022; 7: 554–568. <http://doi.org/10.1530/EOR-22-0004>.
- [2] Nagai M, Aoyama T, Ito A, Iijima H, Yamaguchi S, Tajino J, *et al.* Contributions of biarticular myogenic components to the limitation of the range of motion after immobilization of rat knee joint. *BMC Musculoskeletal Disorders*. 2014; 15: 224. <http://doi.org/10.1186/1471-2474-15-224>.
- [3] Usher KM, Zhu S, Mavropalias G, Carrino JA, Zhao J, Xu J. Pathological mechanisms and therapeutic outlooks for arthrofibrosis. *Bone Research*. 2019; 7: 9. <https://doi.org/10.1038/s41413-019-0047-x>.
- [4] Zhou Y, Zhang QB, Zhong HZ, Liu Y, Li J, Lv H, *et al.* Rabbit Model of Extending Knee Joint Contracture: Progression of Joint Motion Restriction and Subsequent Joint Capsule Changes after Immobilization. *The Journal of Knee Surgery*. 2020; 33: 15–21. <http://doi.org/10.1055/s-0038-1676502>.
- [5] Zhou CX, Wang F, Zhou Y, Fang QZ, Zhang QB. Formation process of extension knee joint contracture following external immobilization in rats. *World Journal of Orthopedics*. 2023; 14: 669–681. <https://doi.org/10.5312/wjo.v14.i9.669>.
- [6] Qin H, Du L, Luo Z, He Z, Wang Q, Chen S, *et al.* The therapeutic effects of low-intensity pulsed ultrasound in musculoskeletal soft tissue injuries: Focusing on the molecular mechanism. *Frontiers in Bioengineering and Biotechnology*. 2022; 10: 1080430. <https://doi.org/10.3389/fbioe.2022.1080430>.
- [7] Itaya N, Yabe Y, Hagiwara Y, Kanazawa K, Koide M, Sekiguchi T, *et al.* Effects of Low-Intensity Pulsed Ultrasound for Preventing Joint Stiffness in Immobilized Knee Model in Rats. *Ultrasound in Medicine & Biology*. 2018; 44: 1244–1256. <http://doi.org/10.1016/j.ultrasmedbio.2018.02.002>.
- [8] Hu R, Yang ZY, Li YH, Zhou Z. LIPUS Promotes Endothelial Differentiation and Angiogenesis of Periodontal Ligament Stem Cells by Activating Piezo1. *International Journal of Stem Cells*. 2022; 15: 372–383. <http://doi.org/10.15283/ijsc.22024>.
- [9] Liao B, Guan M, Tan Q, Wang G, Zhang R, Huang J, *et al.* Low-intensity pulsed ultrasound inhibits fibroblast-like synoviocyte proliferation and reduces synovial fibrosis by regulating Wnt/ $\beta$ -catenin signaling. *Journal of Orthopaedic Translation*. 2021; 30: 41–50. <http://doi.org/10.1016/j.jot.2021.08.002>.
- [10] Yang T, Liang C, Chen L, Li J, Geng W. Low-Intensity Pulsed Ultrasound Alleviates Hypoxia-Induced Chondrocyte Damage in Temporomandibular Disorders by Modulating the Hypoxia-Inducible Factor Pathway. *Frontiers in Pharmacology*. 2020; 11: 689. <https://doi.org/10.3389/fphar.2020.00689>.
- [11] Nakamura T, Fujihara S, Katsura T, Yamamoto K, Inubushi T, Tanimoto K, *et al.* Effects of low-intensity pulsed ultrasound on the expression and activity of hyaluronan synthase and hyaluronidase in IL-1 $\beta$ -stimulated synovial cells. *Annals of Biomedical Engineering*. 2010; 38: 3363–3370. <https://doi.org/10.1007/s10439-010-0104-5>.
- [12] Zhou T, Zhou CX, Zhang QB, Wang F, Zhou Y. LIPUS Alleviates Knee Joint Capsule Fibrosis in Rabbits by Regulating SOD/ROS Dynamics and Inhibiting the TGF- $\beta$ 1/Smad Signaling Pathway. *Ultrasound in Medicine & Biology*. 2023; 49: 2510–2518. <https://doi.org/10.1016/j.ultrasmedbio.2023.08.014>.
- [13] Aibara Y, Nakashima A, Kawano K, Yusoff FM, Mizuki F, Kishimoto S, *et al.* Daily Low-intensity Pulsed Ultrasound Ameliorates Renal Fibrosis and Inflammation in Experimental Hypertensive and Diabetic Nephropathy. *Hypertension*. 2020; 76: 1906–1914. <http://doi.org/10.1161/HYPERTENSIONAHA.120.15237>.
- [14] Monma Y, Shindo T, Eguchi K, Kurosawa R, Kagaya Y, Ikumi Y, *et al.* Low-intensity pulsed ultrasound ameliorates cardiac diastolic dysfunction in mice: a possible novel therapy for heart failure with preserved left ventricular ejection fraction. *Cardiovascular Research*.

- 2021; 117: 1325–1338. <http://doi.org/10.1093/cvr/cvaa221>.
- [15] Feng S, Tang D, Wang Y, Li X, Bao H, Tang C, *et al.* The mechanism of ferroptosis and its related diseases. *Molecular Biomedicine*. 2023; 4: 33. <https://doi.org/10.1186/s43556-023-00142-2>.
- [16] Fu Y, Zhou X, Wang L, Fan W, Gao S, Zhang D, *et al.* Salvianolic acid B attenuates liver fibrosis by targeting Ecm1 and inhibiting hepatocyte ferroptosis. *Redox Biology*. 2024; 69: 103029. <http://doi.org/10.1016/j.redox.2024.103029>.
- [17] Li XT, Song JW, Zhang ZZ, Zhang MW, Liang LR, Miao R, *et al.* Sirtuin 7 mitigates renal ferroptosis, fibrosis and injury in hypertensive mice by facilitating the KLF15/Nrf2 signaling. *Free Radical Biology & Medicine*. 2022; 193: 459–473. <http://doi.org/10.1016/j.freeradbiomed.2022.10.320>.
- [18] Pei Z, Qin Y, Fu X, Yang F, Huo F, Liang X, *et al.* Inhibition of ferroptosis and iron accumulation alleviates pulmonary fibrosis in a bleomycin model. *Redox Biology*. 2022; 57: 102509. <http://doi.org/10.1016/j.redox.2022.102509>.
- [19] Zhang Z, Tang J, Song J, Xie M, Liu Y, Dong Z, *et al.* Elabela alleviates ferroptosis, myocardial remodeling, fibrosis and heart dysfunction in hypertensive mice by modulating the IL-6/STAT3/GPX4 signaling. *Free Radical Biology & Medicine*. 2022; 181: 130–142. <http://doi.org/10.1016/j.freeradbiomed.2022.01.020>.
- [20] Liu T, Jiang L, Tavana O, Gu W. The Deubiquitylase OTUB1 Mediates Ferroptosis via Stabilization of SLC7A11. *Cancer Research*. 2019; 79: 1913–1924. <http://doi.org/10.1158/0008-5472.CA N-18-3037>.
- [21] Gong Y, Wang N, Liu N, Dong H. Lipid Peroxidation and GPX4 Inhibition Are Common Causes for Myofibroblast Differentiation and Ferroptosis. *DNA and Cell Biology*. 2019; 38: 725–733. <http://doi.org/10.1089/dna.2018.4541>.
- [22] Ouyang ZQ, Shao LS, Wang WP, Ke TF, Chen D, Zheng GR, *et al.* Low intensity pulsed ultrasound ameliorates Adriamycin-induced chronic renal injury by inhibiting ferroptosis. *Redox Report: Communications in Free Radical Research*. 2023; 28: 2251237. <http://doi.org/10.1080/13510002.2023.2251237>.
- [23] Tang B, Yan R, Zhu J, Cheng S, Kong C, Chen W, *et al.* Integrative analysis of the molecular mechanisms, immunological features and immunotherapy response of ferroptosis regulators across 33 cancer types. *International Journal of Biological Sciences*. 2022; 18: 180–198. <http://doi.org/10.7150/ijbs.64654>.
- [24] Zhang BB, Xu L, Zhang QB, Wang Y, Chen C, Zhang JN, *et al.* Anti-fibrosis effect and its mechanism of atracylenolide III on post-traumatic extending knee joint contracture in rats. *Experimental Gerontology*. 2025; 201: 112708. <http://doi.org/10.1016/j.exger.2025.112708>.
- [25] Zhang X, Li LX, Ding H, Torres VE, Yu C, Li X. Ferroptosis Promotes Cyst Growth in Autosomal Dominant Polycystic Kidney Disease Mouse Models. *Journal of the American Society of Nephrology: JASN*. 2021; 32: 2759–2776. <http://doi.org/10.1681/ASN.2021040460>.
- [26] Gan D, Jin X, Wang X, Tao C, Yan Q, Jia Q, *et al.* Pathological progress and remission strategies of osteoarthritic lesions caused by long-term joint immobilization. *Arthritis Research & Therapy*. 2023; 25: 237. <https://doi.org/10.1186/s13075-023-03223-3>.
- [27] Sasabe R, Sakamoto J, Goto K, Honda Y, Kataoka H, Nakano J, *et al.* Effects of joint immobilization on changes in myofibroblasts and collagen in the rat knee contracture model. *Journal of Orthopaedic Research: Official Publication of the Orthopaedic Research Society*. 2017; 35: 1998–2006. <http://doi.org/10.1002/jor.23498>.
- [28] Wang F, Zhang QB, Zhou Y, Chen S, Huang P, Liu Y, *et al.* The mechanisms and treatments of muscular pathological changes in immobilization-induced joint contracture: A literature review. *Chinese Journal of Traumatology = Zhonghua Chuang Shang Za Zhi/Chinese Medical Association*. 2019; 22: 93–98. <http://doi.org/10.1016/j.cjtee.2019.02.001>.
- [29] Wang F, Zhou T, Zhou CX, Zhang QB, Wang H, Zhou Y. The worsening of skeletal muscle atrophy induced by immobilization at the early stage of remobilization correlates with BNIP3-dependent mitophagy. *BMC Musculoskeletal Disorders*. 2023; 24: 632. <https://doi.org/10.1186/s12891-023-06759-2>.
- [30] Yuan H, Wang K, Zhang QB, Wang F, Zhou Y. The effect of extracorporeal shock wave on joint capsule fibrosis based on A2AR-Nrf2/HO-1 pathway in a rat extending knee immobilization model. *Journal of Orthopaedic Surgery and Research*. 2023; 18: 930. <https://doi.org/10.1186/s13018-023-04420-1>.
- [31] Bayram B, Limberg AK, Salib CG, Bettencourt JW, Trousdale WH, Lewallen EA, *et al.* Molecular pathology of human knee arthrofibrosis defined by RNA sequencing. *Genomics*. 2020; 112: 2703–2712. <http://doi.org/10.1016/j.ygeno.2020.03.004>.
- [32] Jiang X, Savchenko O, Li Y, Qi S, Yang T, Zhang W, *et al.* A Review of Low-Intensity Pulsed Ultrasound for Therapeutic Applications. *IEEE Transactions on Bio-Medical Engineering*. 2019; 66: 2704–2718. <http://doi.org/10.1109/TBME.2018.2889669>.
- [33] Xu T, Gu J, Li C, Guo X, Tu J, Zhang D, *et al.* Low-intensity pulsed ultrasound suppresses proliferation and promotes apoptosis via p38 MAPK signaling in rat visceral preadipocytes. *American Journal of Translational Research*. 2018; 10: 948–956.
- [34] Duan H, Chen S, Mai X, Fu L, Huang L, Xiao L, *et al.* Low-intensity pulsed ultrasound (LIPUS) promotes skeletal muscle regeneration by regulating PGC-1 $\alpha$ /AMPK/GLUT4 pathways in satellite cells/myoblasts. *Cellular Signalling*. 2024; 117: 111097. <https://doi.org/10.1016/j.cellsig.2024.111097>.
- [35] Hill GE, Fenwick S, Matthews BJ, Chivers RA, Southgate J. The effect of low-intensity pulsed ultrasound on repair of epithelial cell monolayers *in vitro*. *Ultrasound in Medicine & Biology*. 2005; 31: 1701–1706. <http://doi.org/10.1016/j.ultrasmedbio.2005.08.001>.
- [36] Mori T, Kawara S, Shinozaki M, Hayashi N, Kakinuma T, Igarashi A, *et al.* Role and interaction of connective tissue growth factor with transforming growth factor-beta in persistent fibrosis: A mouse fibrosis model. *Journal of Cellular Physiology*. 1999; 181: 153–159. [http://doi.org/10.1002/\(SICI\)1097-4652\(199910\)181:1<153::AID-JCP16>3.0.CO;2-K](http://doi.org/10.1002/(SICI)1097-4652(199910)181:1<153::AID-JCP16>3.0.CO;2-K).
- [37] Zhang Y, Wang Z, Zong C, Gu X, Fan S, Xu L, *et al.* Platelet-rich plasma attenuates the severity of joint capsule fibrosis following post-traumatic joint contracture in rats. *Frontiers in Bioengineering and Biotechnology*. 2023; 10: 1078527. <https://doi.org/10.3389/fbioe.2022.1078527>.
- [38] Fang J, Shu S, Dong H, Yue X, Piao J, Li S, *et al.* Histone deacetylase 6 controls cardiac fibrosis and remodelling through the modulation of TGF- $\beta$ 1/Smad2/3 signalling in post-infarction mice. *Journal of Cellular and Molecular Medicine*. 2024; 28: e70063. <https://doi.org/10.1111/jcmm.70063>.
- [39] Lei H, Xin H, Guan R, Xu Y, Li H, Tian W, *et al.* Low-intensity Pulsed Ultrasound Improves Erectile Function in Streptozotocin-induced Type I Diabetic Rats. *Urology*. 2015; 86: 1241.e11–1241.e18. <http://doi.org/10.1016/j.urology.2015.07.026>.
- [40] Kitagawa T, Kawahata H, Aoki M, Kudo S. Inhibitory effect of low-intensity pulsed ultrasound on the fibrosis of the infrapatellar fat pad through the regulation of HIF-1 $\alpha$  in a carrageenan-induced knee osteoarthritis rat model. *Biomedical Reports*. 2022; 17: 79. <https://doi.org/10.3892/br.2022.1562>.
- [41] Hu C, Zhang QB, Wang F, Wang H, Zhou Y. The effect of extracorporeal shock wave on joint capsule fibrosis in rats with knee extension contracture: a preliminary study. *Connective Tissue Research*. 2023; 64: 469–478. <http://doi.org/10.1080/03008207.2023.2217254>.
- [42] Xu Z, Li S, Wan L, Hu J, Lu H, Zhang T. Role of low-intensity pulsed ultrasound in regulating macrophage polarization to accelerate tendon-bone interface repair. *Journal of Orthopaedic Research: Official Publication of the Orthopaedic Research Society*. 2023; 41: 919–929. <http://doi.org/10.1002/jor.25454>.
- [43] Duffield JS, Forbes SJ, Constandinou CM, Clay S, Partolina M,

- Vuthoori S, *et al.* Selective depletion of macrophages reveals distinct, opposing roles during liver injury and repair. *The Journal of Clinical Investigation*. 2005; 115: 56–65. <http://doi.org/10.1172/JC122675>.
- [44] Chen B, Huang S, Su Y, Wu YJ, Hanna A, Brickshawana A, *et al.* Macrophage Smad3 Protects the Infarcted Heart, Stimulating Phagocytosis and Regulating Inflammation. *Circulation Research*. 2019; 125: 55–70. <http://doi.org/10.1161/CIRCRESAHA.119.315069>.
- [45] Della Latta V, Cecchetti A, Del Ry S, Morales MA. Bleomycin in the setting of lung fibrosis induction: From biological mechanisms to counteractions. *Pharmacological Research*. 2015; 97: 122–130. <http://doi.org/10.1016/j.phrs.2015.04.012>.
- [46] Castello L, Froio T, Maina M, Cavallini G, Biasi F, Leonarduzzi G, *et al.* Alternate-day fasting protects the rat heart against age-induced inflammation and fibrosis by inhibiting oxidative damage and NF- $\kappa$ B activation. *Free Radical Biology & Medicine*. 2010; 48: 47–54. <http://doi.org/10.1016/j.freeradbiomed.2009.10.003>.
- [47] Cheng H, Feng D, Li X, Gao L, Tang S, Liu W, *et al.* Iron deposition-induced ferroptosis in alveolar type II cells promotes the development of pulmonary fibrosis. *Biochimica et Biophysica Acta. Molecular Basis of Disease*. 2021; 1867: 166204. <http://doi.org/10.1016/j.bbadis.2021.166204>.
- [48] Wang J, Wang Y, Liu Y, Cai X, Huang X, Fu W, *et al.* Ferroptosis, a new target for treatment of renal injury and fibrosis in a 5/6 nephrectomy-induced CKD rat model. *Cell Death Discovery*. 2022; 8: 127. <https://doi.org/10.1038/s41420-022-00931-8>.
- [49] Lightbody G, Haberland V, Browne F, Taggart L, Zheng H, Parkes E, *et al.* Review of applications of high-throughput sequencing in personalized medicine: barriers and facilitators of future progress in research and clinical application. *Briefings in Bioinformatics*. 2019; 20: 1795–1811. <http://doi.org/10.1093/bib/bby051>.
- [50] Zhu B, Ni Y, Gong Y, Kang X, Guo H, Liu X, *et al.* Formononetin ameliorates ferroptosis-associated fibrosis in renal tubular epithelial cells and in mice with chronic kidney disease by suppressing the Smad3/ATF3/SLC7A11 signaling. *Life Sciences*. 2023; 315: 121331. <http://doi.org/10.1016/j.lfs.2022.121331>.
- [51] He X, Xiong Y, Liu Y, Li Y, Zhou H, Wu K. Ferrostatin-1 inhibits ferroptosis of vascular smooth muscle cells and alleviates abdominal aortic aneurysm formation through activating the SLC7A11/GPX4 axis. *FASEB Journal: Official Publication of the Federation of American Societies for Experimental Biology*. 2024; 38: e23401. <https://doi.org/10.1096/fj.202300198RRR>.
- [52] Li Q, Peng F, Yan X, Chen Y, Zhou J, Wu S, *et al.* Inhibition of SLC7A11-GPX4 signal pathway is involved in aconitine-induced ferroptosis *in vivo* and *in vitro*. *Journal of Ethnopharmacology*. 2023; 303: 116029. <http://doi.org/10.1016/j.jep.2022.116029>.
- [53] Dolma S, Lessnick SL, Hahn WC, Stockwell BR. Identification of genotype-selective antitumor agents using synthetic lethal chemical screening in engineered human tumor cells. *Cancer Cell*. 2003; 3: 285–296. [http://doi.org/10.1016/s1535-6108\(03\)00050-3](http://doi.org/10.1016/s1535-6108(03)00050-3).
- [54] Ortiz-Rodríguez JM, Martín-Cano FE, Gaitskell-Phillips G, Silva A, Tapia JA, Gil MC, *et al.* The SLC7a11: sperm mitochondrial function and non-canonical glutamate metabolism. *Reproduction: The Official Journal of the Society for the Study of Fertility*. 2020; 160: 803–818. <http://doi.org/10.1530/REP-20-0181>.

**Editor's note:** The Scientific Editor responsible for this paper was Chris Evans.

**Received:** 31st March 2025; **Accepted:** 15th September 2025; **Published:** 28th November 2025